Numerical Simulation of Particle-Laden Plane Mixing Layer by Three-Dimensional Vortex Method*

Hisanori YAGAMI** and Tomomi UCHIYAMA***

A plane air mixing layer loaded with spherical glass particles is simulated by the three-dimensional vortex method proposed for gas-particle two-phase free turbulent flow by the authors in a prior study. The vortex method computes simultaneously the behavior of vortex element and the particle motion by the Lagrangian approach. It is demonstrated that the simulated particle distribution, mean velocity and fluctuating velocity agree with the measurement and that the vortex method is indeed applicable to the analysis of particle-laden plane mixing layer. The change in the vortical structure due to the loaded particles is also discussed.

Key Words: Numerical Analysis, Multi-Phase Flow, Three-Dimensional Flow, Mixing Layer, Gas-Particle Two-Phase Flow, Vortical Structure, Vortex Method

1. Introduction

Free turbulent gas flows loaded with small solid particles are observed in various industrial devices, such as pulverized-coal combustors, solid rocket engines and chemical reactors. The relation between the organized large-scale eddies and the particle behavior has thus far received much attention. The particle velocity and number density were measured in a plane mixing layer[1], a jet[2] and a wake[3]. A Direct Numerical Simulation[4] and a Large Eddy Simulation[5] on two-phase jets were also performed to supplement the experimental work, and the effect of particle on the gas flow was explored.

It should be noted that vortex methods have been usefully applied to analyze single-phase flows[6),(7]. They can calculate directly the development of vortical structure, such as the formation and deformation of vortices, by tracing the motion of the vortex elements having vorticity through the Lagrangian approach. Therefore, they have been favorably applied to free turbulent flows, in which the organized large-scale eddies play a dominant role.

One of the authors[8] proposed a two-dimensional vortex method for gas-particle two-phase free turbulent flow. The method was applied to plane mixing layers[9),(10], a slit nozzle jet[11] and a wake flow behind a plate[12] to analyze the effect of particle on the flow development as well as the relation between the large-scale eddy and the particle motion. The vortex method was also employed to simulate the particulate jet induced by particles falling in an unbounded quiescent air[13]. Uchiyama and Fukase[14] proposed a three-dimensional vortex method for gas-particle two-phase free turbulent flow. The method was applied to simulate an air jet loaded with glass particles[14)–(16]. The simulations demonstrated that the air turbulent modulations due to the particle agree well with the measurement. The vortex method was also successfully employed to compute the particulate jet induced by falling particles[17].

In this study, a plane air mixing layer loaded with glass particles is simulated by the above-mentioned three-dimensional vortex method. It is demonstrated that the simulated particle distribution, mean velocity and fluctuating velocity agree with the measurement and that the vortex method is indeed applicable to the analysis of particle-laden plane mixing layer. The change in the vortical structure due to the loaded particles is also discussed.

Nomenclature

d : particle diameter
$\boldsymbol{F}_D$: force exerted by particle acting on gas-phase per unit volume
$\boldsymbol{f}_D$: drag force acting on particle
$\boldsymbol{g}$: gravitational constant
$\boldsymbol{l}$: length vector of vortex element
N_v : number of vortex elements in computational region

* Received 15th February, 2006 (No. 06-4044)
** Graduate School of Information Science, Nagoya University, Furo-cho, Chikusa-ku, Nagoya 464–8601, Japan
*** EcoTopia Science Institute, Nagoya University, Furo-cho, Chikusa-ku, Nagoya 464–8603, Japan.
E-mail: uchiyama@is.nagoya-u.ac.jp

p : pressure
t : time
U_1 : gas velocity of higher velocity stream
U_2 : gas velocity of lower velocity stream
U_a : average velocity $=(U_1+U_2)/2$
$\boldsymbol{u}$: velocity
$\boldsymbol{u}'$: fluctuating velocity
$\overline{\boldsymbol{u}}$: mean velocity
x, y, z : orthogonal coordinates
Γ : circulation
$\boldsymbol{\gamma}$: vortex strength
$y_{0.5}$: location at which $\overline{\boldsymbol{u}}=U_a$
Δt : time increment
ΔU : velocity difference $=U_1-U_2$
θ_x : momentum thickness
ν : kinematic viscosity
ρ : density
σ : core radius of vortex element
$\boldsymbol{\omega}$: vorticity $=\nabla\times\boldsymbol{u}_g$

Subscripts

0 : potential flow
g : gas
p : particle

2. Basic Equations

2.1 Assumptions

The following assumptions are employed for the simulation.

(1) The gas-phase is incompressible.
(2) The particle density is much larger than the gas.
(3) The particle has a spherical shape with uniform diameter.
(4) The collision between the particles is negligible.

2.2 Governing equations

The conservation equations for the mass and momentum of the gas-phase are expressed as follows under the assumption (1):

$$\nabla\cdot\boldsymbol{u}_g=0 \tag{1}$$

$$\frac{\partial\boldsymbol{u}_g}{\partial t}+(\boldsymbol{u}_g\cdot\nabla)\boldsymbol{u}_g=-\frac{1}{\rho_g}\nabla p+\nu\nabla^2\boldsymbol{u}_g-\frac{1}{\rho_g}\boldsymbol{F}_D \tag{2}$$

where $\boldsymbol{F}_D$ is the force exerted by the particle acting on the gas-phase per unit volume.

Using the assumption (2), the dominant forces on the particle are the drag and gravitational forces, while the virtual mass force, the Basset force and the pressure gradient force are negligible[18]. The lift force is neglected with reference to the studies simulating the particle motion in a jet[19], a plane wake[20] and mixing layers[18),21]. Consequently, the equation of motion for a particle (mass m) is written as:

$$m\frac{d\boldsymbol{u}_p}{dt}=\boldsymbol{f}_D+m\boldsymbol{g} \tag{3}$$

where the drag force $\boldsymbol{f}_D$ is given by the following from the assumption (3):

$$\boldsymbol{f}_D=(\pi d^2\rho_g/8)C_D|\boldsymbol{u}_g-\boldsymbol{u}_p|(\boldsymbol{u}_g-\boldsymbol{u}_p) \tag{4}$$

Here, d is the particle diameter and the drag coefficient C_D is estimated as[22]:

$$C_D=(24/Re_p)(1+0.15Re_p^{0.687}) \tag{5}$$

where $Re_p=d|\boldsymbol{u}_g-\boldsymbol{u}_p|/\nu$.

For the simultaneous calculation of Eqs. (1)–(3), a vortex method is used to solve Eqs. (1) and (2), and the Lagrangian approach is applied to Eq. (3).

3. Numerical Method

3.1 Discretization of gas vorticity field by vortex element

When taking the curl of Eq. (2) and substituting Eq. (1) into the resultant equation, the vorticity equation for the gas-phase is derived:

$$\frac{D\boldsymbol{\omega}}{Dt}=(\boldsymbol{\omega}\cdot\nabla)\boldsymbol{u}_g+\nu\nabla^2\boldsymbol{\omega}-\frac{1}{\rho_g}\nabla\times\boldsymbol{F}_D \tag{6}$$

where $\boldsymbol{\omega}$ is the vorticity for the gas-phase.

The gas velocity $\boldsymbol{u}_g$ at $\boldsymbol{x}$ is given by the Biot-Savart equation:

$$\boldsymbol{u}_g(\boldsymbol{x})=-\frac{1}{4\pi}\int\frac{(\boldsymbol{x}-\boldsymbol{x}')\times\boldsymbol{\omega}(\boldsymbol{x}')}{|\boldsymbol{x}-\boldsymbol{x}'|^3}dV(\boldsymbol{x}')+\boldsymbol{u}_{g0} \tag{7}$$

where $\boldsymbol{u}_{g0}$ denotes the velocity of potential flow.

The vorticity field is discretized by vortex elements. Various models have been proposed for the element in the three-dimensional vortex method. The present analysis employs a blob model[6], which is frequently used to solve engineering problems. The vortex element has a cylindrical shape as illustrated in Fig. 1, while the vorticity distribution is spherical with a finite core radius.

When the vortex element α at $\boldsymbol{x}^\alpha$ is supposed to have a core radius σ_α, the vorticity at $\boldsymbol{x}$ induced by the vortex element is expressed by the following equation:

$$\boldsymbol{\omega}^\alpha(\boldsymbol{x})=\frac{\boldsymbol{\gamma}^\alpha}{\sigma_\alpha^3}f\left(\frac{|\boldsymbol{x}-\boldsymbol{x}^\alpha|}{\sigma_\alpha}\right) \tag{8}$$

Here, $f(\varepsilon)$ is the core distribution function, and $\boldsymbol{\gamma}^\alpha$ is the strength of vortex element expressed as:

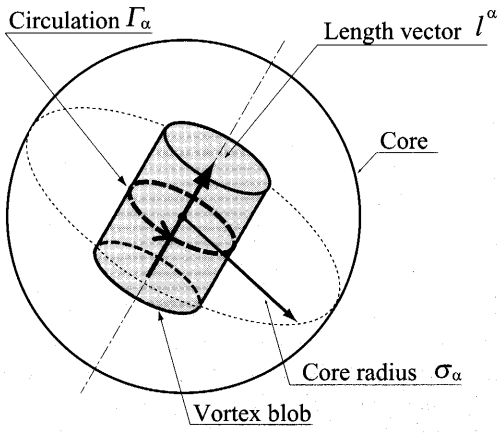

Fig. 1 Vortex element

$$\boldsymbol{\gamma}^{\alpha} = \Gamma_{\alpha} \boldsymbol{l}^{\alpha} \tag{9}$$

where Γ_{α} and $\boldsymbol{l}^{\alpha}$ are the circulation and length vector of vortex element respectively, as indicated in Fig. 1.

A variety of functions have been proposed for $f(\varepsilon)$. The following equation proposed by Winckelmans-Leonard[6] is employed in this analysis.

$$f(\varepsilon) = \frac{15}{8\pi(\varepsilon^2+1)^{7/2}} \tag{10}$$

When the vorticity field is discretized into a set of N_v vortex elements, the velocity $\boldsymbol{u}_g(\boldsymbol{x})$ is given by the following equation derived from Eqs. (7) and (8):

$$\boldsymbol{u}_g(\boldsymbol{x}) = -\frac{1}{4\pi}\sum_{\alpha=1}^{N_v} \frac{(\boldsymbol{x}-\boldsymbol{x}^{\alpha})\times\boldsymbol{\gamma}^{\alpha}}{|\boldsymbol{x}-\boldsymbol{x}^{\alpha}|^3} g\left(\frac{|\boldsymbol{x}-\boldsymbol{x}^{\alpha}|}{\sigma_{\alpha}}\right) + \boldsymbol{u}_{g0} \tag{11}$$

where the function $g(\varepsilon)$ is determined as:

$$g(\varepsilon) = 4\pi \int_0^{\varepsilon} f(\zeta)\zeta^2 d\zeta \tag{12}$$

3.2 Release and convection of vortex element

The vortex elements adjacent to the tip of splitter plate are released into the mixing region at a time interval Δt_v to express the velocity shear layer. The vortex element convects with the fluid velocity at its center given by Eq. (7). The Lagrangian method is applied to calculate the convection:

$$\frac{d\boldsymbol{x}^{\alpha}}{dt} = \boldsymbol{u}_g(\boldsymbol{x}^{\alpha}) \tag{13}$$

When Eq. (6) is rewritten in the Lagrangian coordinates, it is found that the vorticity of vortex element varies with the lapse of time due to the change in the length of vortex element, the viscous diffusion, and the force exerted by the loaded particles. These changes are computed simultaneously with the Lagrangian calculation of Eq. (13), as explained in the following.

3.3 Change in vorticity due to stretch and contraction of vortex element

The time evolution in the vorticity owing to the stretch and contraction of the vortex element is calculated from the Lagrangian expression of Eq. (6) omitting the viscous diffusion and particle terms:

$$\frac{d\boldsymbol{\omega}}{dt} = (\boldsymbol{\omega}\cdot\nabla)\boldsymbol{u}_g \tag{14}$$

Substituting Eqs. (7) and (8) into Eq. (14), the time rate of change in $\boldsymbol{\gamma}^{\alpha}$ is derived:

$$\frac{d\boldsymbol{\gamma}^{\alpha}}{dt} = \frac{1}{4\pi}\sum_{\beta=1}^{N_v} \frac{1}{\sigma_{\beta}^3}\left\{-\frac{g(\zeta)}{\zeta^3}\boldsymbol{\gamma}^{\alpha}\times\boldsymbol{\gamma}^{\beta} + \frac{1}{\sigma_{\beta}^2}\left[-\frac{1}{\zeta}\frac{d}{d\zeta}\left(\frac{g(\zeta)}{\zeta^3}\right)\right] \times\left[\boldsymbol{\gamma}^{\alpha}\cdot(\boldsymbol{x}^{\alpha}-\boldsymbol{x}^{\beta})\right]\left[(\boldsymbol{x}^{\alpha}-\boldsymbol{x}^{\beta})\times\boldsymbol{\gamma}^{\beta}\right]\right\} \tag{15}$$

where $\zeta = |\boldsymbol{x}^{\alpha}-\boldsymbol{x}^{\beta}|/\sigma_{\beta}$.

3.4 Change in core radius due to viscosity

The vorticity decreases due to the viscous effect. The decrement is simulated by applying a core spreading method for single-phase flow[23], in which the core radius σ of vortex element is made to increase with the lapse of time. The Lagrangian method is applied to calculate σ:

$$\frac{d\sigma^2}{dt} = 4\nu \tag{16}$$

Equation (16) represents the rate of core spread for an isolated vortex filament in a quiescent fluid. It is derived from the Navier-Stokes equation.

3.5 Change in strength of vortex element due to particle

When substituting Eq. (6) into an equation, derived from the Reynolds transport theorem and Eq. (1), the time rate of change in the strength of vorticity $\boldsymbol{\gamma}$ in any volume is obtained:

$$\frac{D\boldsymbol{\gamma}}{Dt} = -\frac{1}{\rho_g}\int(\nabla\times\boldsymbol{F}_D)dV = -\frac{1}{\rho_g}\int(\boldsymbol{n}\times\boldsymbol{F}_D)dS \tag{17}$$

where $\boldsymbol{n}$ is the unit vector normal to the volume surface, and the stretch-contraction term and the viscous diffusion term are neglected because they are already considered through Eqs. (15) and (16), respectively.

The computational domain is resolved into hexahedral grids. A grid is shown in Fig. 2 (a). If the $\boldsymbol{F}_D$ value is known on every surface of a grid, the time rate of change for $\boldsymbol{\gamma}$, $\Delta\boldsymbol{\gamma}/\Delta t$, in the grid is determined from Eq. (17). For example, the x-component $\Delta\gamma_x/\Delta t$ is written as:

$$\frac{\Delta\gamma_x}{\Delta t} = -\frac{1}{\rho_g}[(F_{Dz}^{B}-F_{Dz}^{A})\Delta S_y + (F_{Dy}^{C}-F_{Dy}^{D})\Delta S_z] \tag{18}$$

where F_{Dz}^{A} is the F_{Dz} value on the surface A, and ΔS_y is the area of a surface normal to the y-axis. In the case in which the number of vortex elements in a grid is n_v, the change in the strength for each vortex element during Δt is supposed to be $\Delta\boldsymbol{\gamma}/n_v$. In the case where there are no vortex elements in the grid, a vortex element with a strength $\Delta\boldsymbol{\gamma}$ is generated at the grid center.

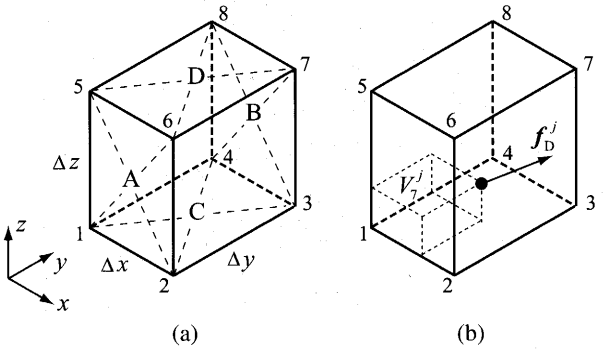

Fig. 2 Computational grid

The $\boldsymbol{F}_D$ value on a grid surface is estimated by using the drag force acting on the particles in the grid, because $\boldsymbol{F}_D$ is the reaction of the drag force. The $\boldsymbol{F}_D$ value on a grid surface in Eq. (18), such as F^A_{Dz}, is estimated by taking the average for the $\boldsymbol{F}_D$ values at four grid points on the surface. It is supposed that the number of particles in a grid cell is n_p and that the drag force $\boldsymbol{f}^j_D$ acts on the jth particle. The $\boldsymbol{F}_D$ value on the grid point β, $\boldsymbol{F}^\beta_D$, is estimated by a volume weighted scheme as:

$$\boldsymbol{F}^\beta_D = \frac{1}{V}\sum_{j=1}^{n_p}\frac{V^j_\beta}{V}\boldsymbol{f}^j_D \quad (\beta = 1,2,\cdots,8) \tag{19}$$

where V is the grid volume, and V^j_β is the volume concerning to the grid point β and the particle, as shown in Fig. 2 (b).

4. Simulation Conditions

A particle-laden plane mixing layer is simulated, which was investigated experimentally by Hishida et al.[1] Figure 3 shows the flow configuration. The streamwise direction is vertical downward. Air streams, having velocities $U_1 = 13$ m/s and $U_2 = 4$ m/s at the high- and low-speed sides of a splitter plate respectively, are introduced to a mixing region. Spherical glass particles with a diameter 135 μm and a density $\rho_p = 2\,590$ kg/m^3 are loaded from the plate tip into the origin of the mixing layer. The particle velocity at the plate tip is 0.9 m/s, and the particle mass loading ratio is 0.13. Wen et al.[21] conducted the experiment on a particle-laden plane mixing layer. They also loaded glass particles from the tip of splitter plate into the mixing layer. It is clarified that the particle motion in free shear flow is chiefly governed by the vortical structure originating from the tip of the splitter plate. The experiments[1],[21] loading the particles from the plate tip investigated successfully the characteristics of the particle-laden plane mixing layer. Therefore, this study chooses the flow measured by Hishida et al.[1] to verify the applicability of the vortex method.

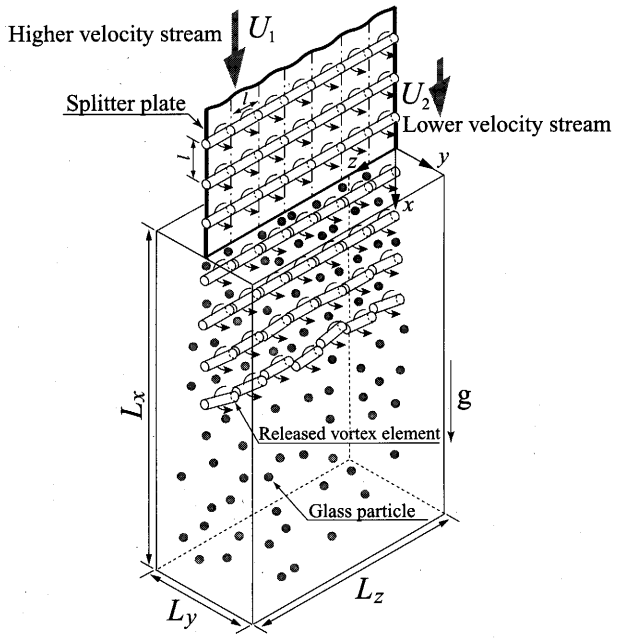

Fig. 3 Configuration of flow field

The computational region downstream of the splitter plate, $L_x = 0.36$ m, $L_y = 0.1$ m and $L_z = 0.18$ m, is resolved into $50 \times 25 \times 25$ hexahedral grids. A periodical boundary condition is applied to the sections at $z = 0$ and L_z. The velocity of potential flow $\boldsymbol{u}_{g0}$ is $(U_1 + U_2)/2$.

The splitter plate is treated as a vortex sheet with reference to the two-dimensional simulation[9],[10], and it is expressed by arranging vortex elements at a space l as shown in Fig. 3. This simulation arranges 234 and 45 vortex elements in the x- and z-directions, respectively. The circulation Γ and length l of the vortex element are given as $(U_1 - U_2)/l$ and $L_z/45$, respectively. The core radius σ is set at $0.5l$ so as to realize the core contact between the neighboring vortex elements.

The vortex elements adjacent to the tip of splitter plate are released into the mixing region at a time interval Δt_v to express the velocity shear layer downstream of the plate. The core radius of the vortex element at the release is $0.5l$. The second-order Adams-Bashforth method is used for the Lagrangian calculation of Eqs. (13) and (15). The time increment Δt for the calculation is 0.47 ms, and $\Delta t_v = \Delta t$. The vortex elements leaving the outlet boundary at $x = L_x$ are excluded from the calculation. To consider the exclusion, the vortex elements are made to convect in the region of $L_x \le x \le L_x + 0.5L_z$ with the strength kept constant.

In the experiment, it is considered that some disturbances are imposed on the air flow at the tip of the splitter plate because of its thickness (1.17 mm). Since this study ignores the thickness, the sinusoidal disturbance is imposed on the releasing position of vortex element (x, y) with reference to the analysis by Inoue[24]:

$$x = A\{1 + \cos[2\pi(z - z_0)/\lambda]\}/2 \tag{20}$$

$$y = A\{1 + \cos[2\pi(z - z_0)/\lambda]\}/2 \tag{21}$$

where the amplitude A is set at the splitter plate thickness, while $z_0 = l/2$ and $\lambda = L_z/3$.

The length vector of vortex element is stretched with the development of the mixing layer, causing deterioration of the spatial resolution. To maintain the resolution, the vortex element is divided into two elements when the length becomes greater than twice its initial value[14)-16),25].

5. Results and Discussions

5.1 Air single-phase mixing layer

First, the vortex method is applied to simulate the air single-phase mixing layer. Figure 4 shows the instanta-

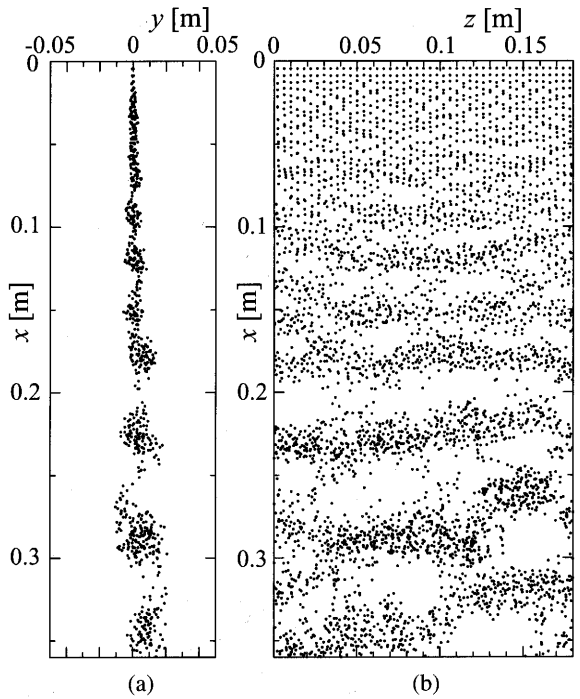

Fig. 4 Instantaneous distribution of vortex element for air single-phase mixing layer

neous distribution of vortex element when the flow develops sufficiently. In Fig. 4 (a), the vortex elements in the region $0.4L_z \le z \le 0.6L_z$ are plotted onto the $x-y$ plane, where the center of each vortex element is indicated by the circular symbol. Figure 4 (b) shows the position for the whole vortex elements projected onto the $z-x$ plane. The vortex elements distribute almost uniformly on a vertical plane at $x \le 0.1$ m, but they form two-dimensional clusters downstream of the region. Each cluster has an axis parallel to the spanwise (z) direction. With increasing streamwise (x) direction, the axis deforms, yielding the three-dimensional distribution of the vortex element.

Figure 5 shows the velocity distribution at the same instant as Fig. 4, where the distribution on the $x-y$ plane at $z = 0.5L_z$ is plotted. The average velocity U_a ($= (U_1 + U_2)/2$) is subtracted to make the vortical structure more understandable. Large-scale eddies occur at $x \ge 0.1$ m. The scale becomes greater with increasing streamwise distance x from the splitter plate, demonstrating that the development of the mixing layer is favorably captured. The large-scale eddies correspond to the clusters of vortex element shown in Fig. 4.

The mean velocity profile is shown in Fig. 6. The nondimensional velocity on four cross-stream sections is plotted. It distributes on a curve at $x \ge 0.1$ m, suggesting that the self-conservation state is simulated. The present result is in good agreement with the measurement[1].

Figure 7 shows the streamwise (x) component of the rms velocity fluctuation. The distribution is in the self-preservation state at $x \ge 0.2$ m in accordance with the measurement[1]. The present result is slightly higher than the measurement. But it seems to be reasonable when compared with the measurement by Oster and Wygnanski[26].

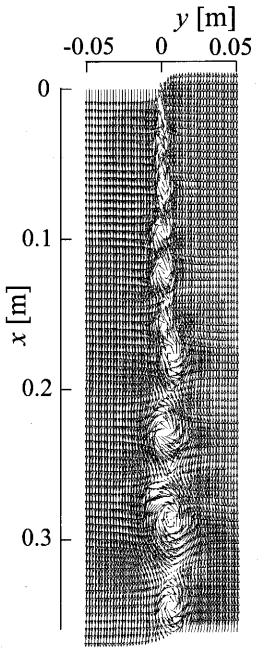

Fig. 5 Instantaneous velocity distribution for air single-phase mixing layer

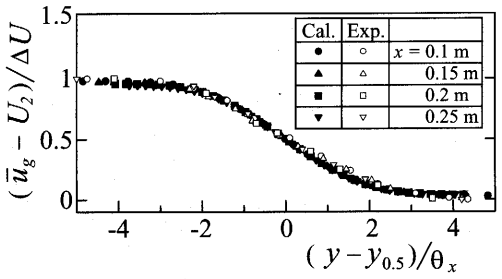

Fig. 6 Mean velocity for air single-phase mixing layer

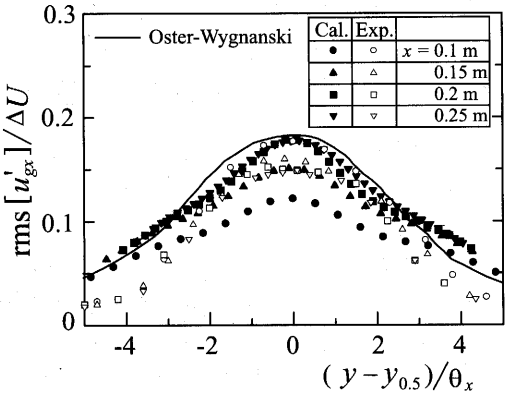

Fig. 7 Streamwise component rms velocity fluctuation for air single-phase mixing layer

5.2 Comparison with measurement

When the particle-laden mixing layer develops sufficiently, the particles distribute as shown in Fig. 8. The par-

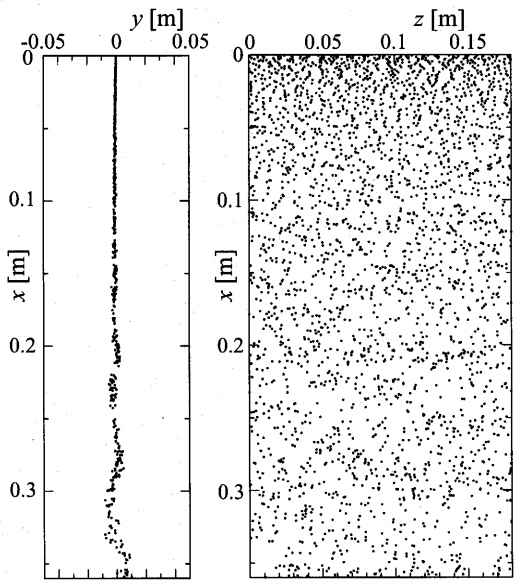

Fig. 8 Particle distribution in two-phase mixing layer

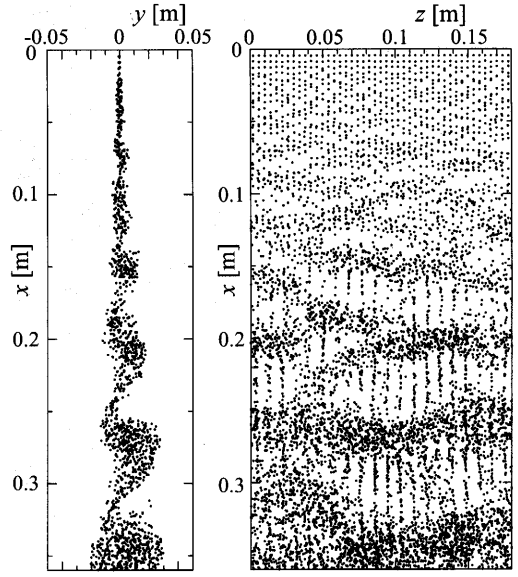

Fig. 9 Distribution of vortex element in two-phase mixing layer

ticles flow almost straight at $x \leq 0.2$ m owing to their large inertia. But they disperse slightly toward the transverse (y) direction due to the large-scale eddies in the downstream region where the mixing layer develops. The particle distribution in the spanwise (z) direction scarcely varies in the streamwise (x) direction.

Figure 9 presents the distribution of vortex element in the same manner as Fig. 4, where the result at the same instant as Fig. 8 is plotted. Since the vortex elements are generated by the particle motion, there are more vortex elements when compared with the air single-phase mixing layer shown in Fig. 4. The number of vortex elements is about 7 200. It is about 1.7 times larger than that for the single-phase mixing layer.

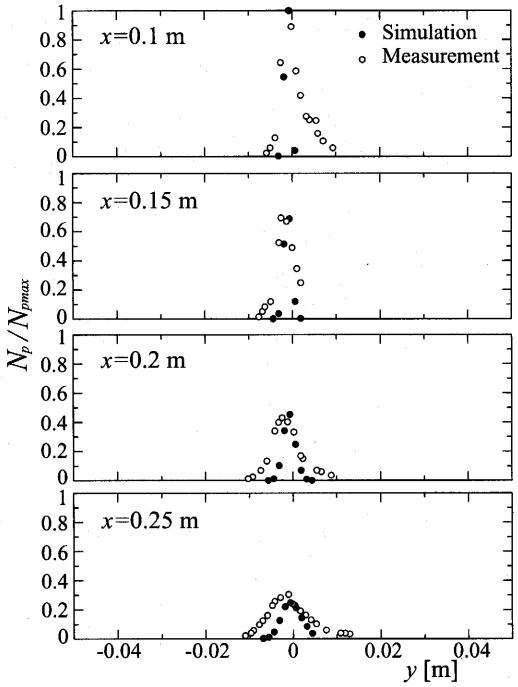

Fig. 10 Particle number density in two-phase mixing layer

Hishida et al.[1] measured the particle distribution, mean velocity and velocity fluctuation. The simulated results are compared with the measurement.

The simulated distribution of particle number density N_p on four cross-stream sections is plotted by the symbol • in Fig. 10, where N_p is normalized by the maximum value N_{pmax} on the section at $x = 0.1$ m. With increasing streamwise distance x from the splitter plate, the particle disperses gradually toward the transverse (y) direction and the maximum value of N_p lessens. The present result is in good agreement with the measurement indicated by the symbol ∘. Regarding the width of distribution in the y-direction, the simulated value is smaller than the measurement. This is because the simulation neglects the collision between the particles.

The streamwise (x) component of the mean velocity for particle $\overline{u}_p$ is plotted by the symbol • in Fig. 11, where the air velocity is superimposed by solid lines. The particle velocity gradually increases with increasing x. But the velocity gradient on each section is not so large. The present result agrees with the measurement plotted by the symbol ∘.

The streamwise component of the rms velocity fluctuation for particle is shown in Fig. 12. It is smaller and flatter than the air velocity fluctuation plotted by the solid line. It is found that the particle cannot fully follow the air turbulent motion due to the large inertia. The present result agrees nearly with the measurement.

5.3 Change in air flow due to particle

The vorticity distribution is presented in Fig. 13. To make the distribution understandable, the iso-surface

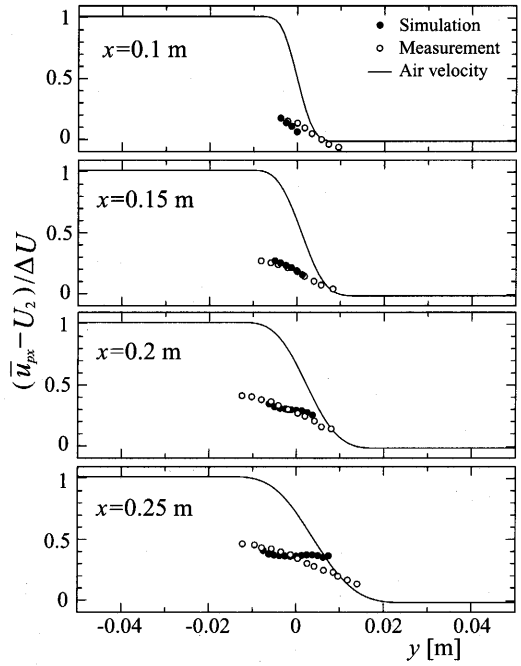

Fig. 11 Mean velocity for particle in two-phase mixing layer

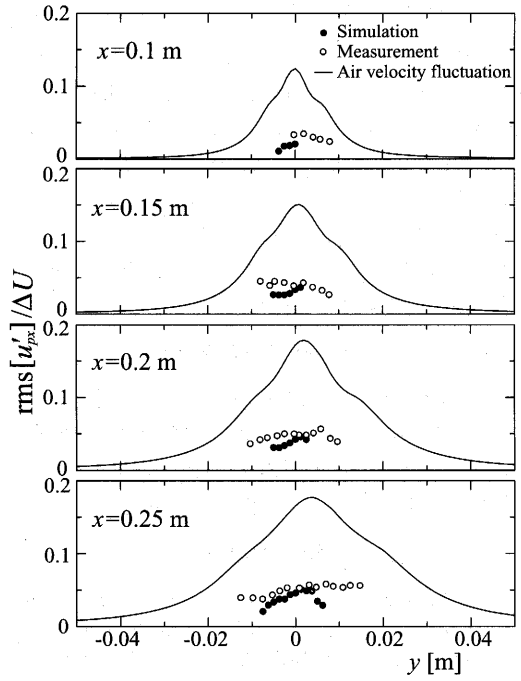

Fig. 12 Streamwise component of rms velocity fluctuation for particle in two-phase mixing layer

$|\omega|/|\omega|_{\max} = 0.2$ is plotted, where $|\omega|_{\max}$ is the maximum value of $|\omega|$. Figure 13 (a) shows the result for the air single-phase mixing layer. The organized large-scale eddies occur at $x = 0.1$ m. They are two-dimensional, and each axis is parallel to the spanwise (z) direction at the region $x \leq 1.6$ m. But the iso-surface varies in the spanwise direction in the downstream region where the mixing layer develops. It is confirmed that the flow becomes three-dimensional. When the initial disturbance

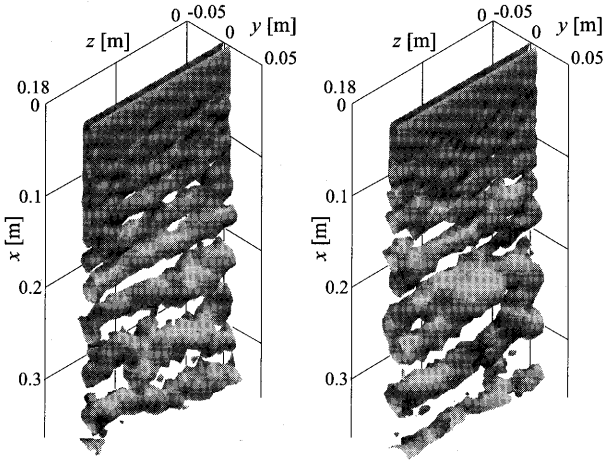

(a) Single-phase mixing layer (b) Two-phase mixing layer ($M = 0.13$)

Fig. 13 Surface of constant magnitude for vorticity $|\omega|/|\omega|_{\max} = 0.2$

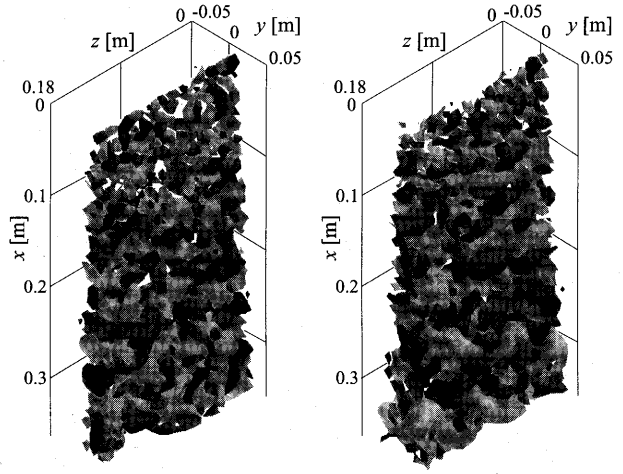

(a) Single-phase mixing layer (b) Two-phase mixing layer

$\omega_x / |\omega_x|_{max} = -0.03$ $\omega_x / |\omega_x|_{max} = 0.03$

Fig. 14 Surfaces of constant magnitude for streamwise vorticity $\omega_x/|\omega_x|_{\max} = \pm 0.03$

given by Eqs. (20) and (21) is not imposed, this three-dimensional feature diminishes markedly. Inoue[24] also analyzed the similar result by the three-dimensional vortex method. These results indicate that the initial disturbance which exists in the experiments on the plane mixing layer greatly affects the transition from the two-dimensional to the three-dimensional flow. Figure 13 (b) shows the iso-surface for the particle-laden mixing layer. The large variation of iso-surface in the spanwise direction appears even at $x = 0.1$ m, and it is greater than that for the single-phase mixing layer in the downstream region. Considering the above-mentioned effect of the initial disturbance on the single-phase mixing layer, such enhancement of the three-dimensional flow feature may be attributable to the disturbance caused by the particles.

Figure 14 shows the distribution of the streamwise

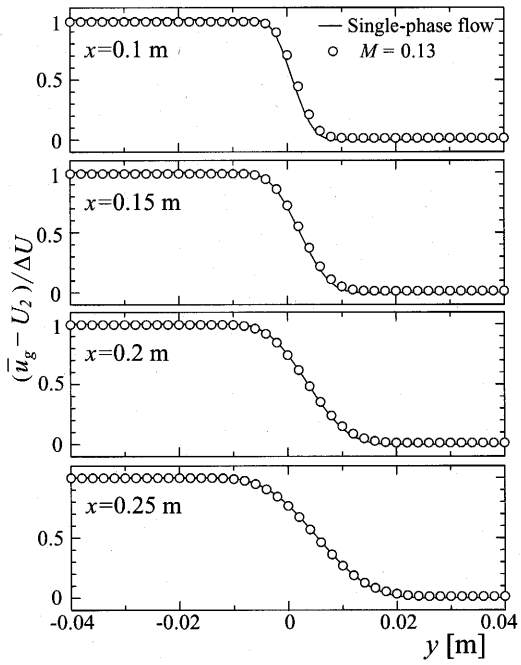

Fig. 15 Mean velocity for air

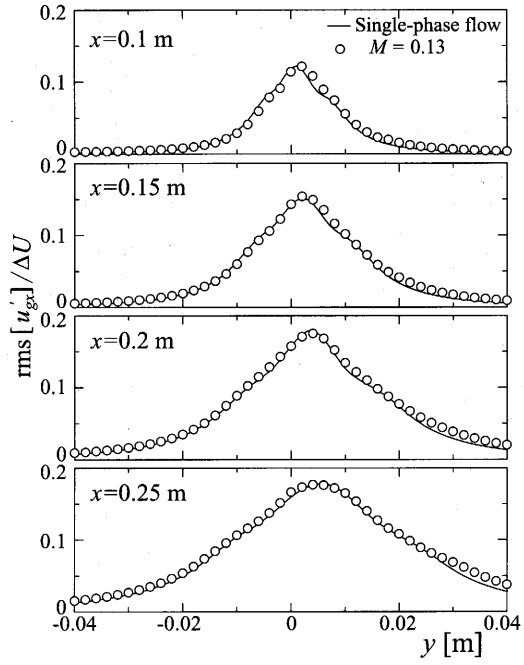

Fig. 16 Streamwise component of rms velocity fluctuation for air

component of vorticity at the same instant as Fig. 13, where the iso-surfaces $\omega_x/|\omega_x|_{max} = \pm 0.03$ are plotted to represent the characteristic feature. Figure 14 (a) indicates the result for the air single-phase mixing layer. Positive and negative vortex tubes exist, and they become entangled. For the particle-laden mixing layer, the streamwise vorticity appears more upstream when compared with the result for the single-phase mixing layer, as found from Fig. 14 (b). This suggests that the three-dimensional air vortical structure occurs more upstream due to the particles. In comparison with the air single-phase mixing layer, ω_x appears over a broader region. Similar change in the air flow due to the loaded particles was also reported in studies simulating gas-particle two-phase jets with the three-dimensional vortex method[14)-16)].

The distribution of mean velocity for air on four cross-stream sections is presented in Fig. 15. On the sections at $x = 0.1$ m and 0.15 m, the velocity increases due to the particles at the low-speed side of the center of the mixing layer ($y = 0$). Such change in the air velocity was also computed by the two-dimensional vortex method[10)].

Figure 16 shows the streamwise component of the rms velocity fluctuation for air. The loaded particles highten the velocity fluctuation.

6. Conclusions

A plane air mixing layer loaded with solid particles is simulated by the three-dimensional vortex method proposed by the authors in a prior study. The mixing layer of velocity ratio 0.3 is loaded with spherical glass particles (diameter, 135 μm; density, 2 590 kg/m^3). The results are summarized as follows:

(1) The particle distribution, mean velocity and fluctuating velocity are in good agreement with the measurement. The vortex method is indeed applicable to the analysis of a particle-laden plane mixing layer.

(2) The simulation captures that the three-dimensional feature of the air flow is enhanced by the loaded particles. It may be attributable to the disturbance caused by the particles.

Acknowledgement

This study was partially supported by a Grant-in-Aid for the 21st Century COE Program "Frontiers of Computational Science" from the Ministry of Education, Culture, Sports, Science and Technology of Japan.

References

(1) Hishida, K., Ando, A. and Maeda, M., Experiments on Particle Dispersion in a Turbulent Mixing Layer, Int. J. Multiphase Flow, Vol.18, No.2 (1992), pp.181–194.

(2) Fleckhaus, D., Hishida, K. and Maeda, M., Effect of Laden Solid Particles on the Turbulent Flow Structure of a Round Free Jet, Exp. Fluids, Vol.5 (1987), pp.323–333.

(3) Yang, Y., Crowe, C.T., Chung, J.N. and Troutt, T.R., Experiments on Particle Dispersion in a Plane Wake, Int. J. Multiphase Flow, Vol.26 (2000), pp.1583–1607.

(4) Yuu, S., Umekage, T. and Tabuchi, M., Direct Numerical Simulation for Three-Dimensional Gas-Solid Two-Phase Jet Using Two-Way Method and Experimental Verification, Trans. Jpn. Soc. Mech. Eng., (in Japanese), Vol.60, No.572, B (1994), pp.1152–1160.

(5) Yuu, S., Ueno, T. and Umekage, T., Numerical Simulation of the High Reynolds Number Slit Nozzle Gas-

Particle Jet Using Subgrid-Scale Coupling Large Eddy Simulation, Chem. Eng. Sci., Vol.56 (2001), pp.4293–4307.

(6) Winckelmans, G.S. and Leonard, A., Contribution to Vortex Particle Methods for the Computation of Three-Dimensional Incompressible Unsteady Flows, J. Comput. Phys., Vol.109 (1993), pp.247–273.

(7) Cottet, G.-H. and Koumoutsakos, P.D., Vortex Method: Theory and Practice, (2000) Cambridge University Press, Cambridge.

(8) Uchiyama, T. and Naruse, M., A Numerical Method for Gas-Solid Two-Phase Free Turbulent Flow Using a Vortex Method, Powder Technol., Vol.119 (2001), pp.206–214.

(9) Uchiyama, T. and Naruse, M., Numerical Simulation of Gas-Particle Two-Phase Mixing Layer by Vortex Method, Powder Technol., Vol.125 (2002), pp.111–121.

(10) Uchiyama, T. and Naruse, M., Numerical Simulation for Gas-Particle Two-Phase Free Turbulent Flow Based on Vortex in Cell Method, Powder Technol., Vol.142 (2004), pp.193–208.

(11) Uchiyama, T. and Naruse, M., Numerical Simulation of Gas-Particle Two-Phase Jet by Vortex Method, Powder Technol., Vol.131 (2003), pp.156–165.

(12) Uchiyama, T. and Yagami, H., Numerical Analysis of Gas-Particle Two-Phase Wake Flow by Vortex Method, Powder Technol., Vol.149 (2005), pp.112–120.

(13) Uchiyama, T., Numerical Analysis of Particulate Jet Generated by Free Falling Particles, Powder Technol., Vol.145 (2004), pp.123–130.

(14) Uchiyama, T. and Fukase, A., Three-Dimensional Vortex Method for Gas-Particle Two-Phase Compound Round Jet, Trans. ASME, J. Fluid Eng., Vol.127 (2005), pp.32–40.

(15) Uchiyama, T. and Fukase, A., Three-Dimensional Vortex Simulation of Particle-Laden Air Jet, Chem. Eng. Sci., Vol.61 (2006), pp.1767–1778.

(16) Uchiyama, T. and Fukase, A., Vortex Simulation of Gas-Particle Two-Phase Compound Round Jet, Powder Technol., (2006), (in press).

(17) Uchiyama, T. and Naruse, M., Three-Dimensional Vortex Simulation for Particulate Jet Generated by Free Falling Particles, Chem. Eng. Sci., Vol.61 (2006), pp.1913–1921.

(18) Chein, R. and Chung, J.N., Effects of Vortex Pairing on Particle Dispersion in Turbulent Shear Flows, Int. J. Multiphase Flow, Vol.13, No.6 (1987), pp.785–802.

(19) Chung, J.N. and Troutt, T.R., Simulation of Particle Dispersion in an Axisymmetric Jet, J. Fluid Mech., Vol.186 (1988), pp.199–222.

(20) Tang, L., Wen, F., Yang, Y., Crowe, C.T., Chung, J.N. and Troutt, T.R., Self-Organizing Particle Dispersion Mechanism in a Plane Wake, Phys. Fluids A, Vol.4, No.10 (1992), pp.2244–2251.

(21) Wen, F., Kamalu, N., Chung, J.N., Crowe, C.T. and Troutt, T.R., Particle Dispersion by Vortex Structures in Plane Mixing Layers, Trans. ASME, J. Fluids Eng., Vol.114, No.6 (1992), pp.657–666.

(22) Schiller, L. and Naumann, A.Z., Uber Die Grundlegenden Berechnungen Bei Der Schwerkraftaufbereitung, Z. Vereines Deutscher Inge., Vol.77 (1933), pp.318–321.

(23) Leonard, A., Vortex Methods for Flow Simulation, J. Comput. Phys., Vol.37 (1980), pp.289–335.

(24) Inoue, O., Vortex Simulation of Spatially Growing Three-Dimensional Mixing Layers, J. AIAA, Vol.27 (1989), pp.1517–1523.

(25) Uchiyama, T., Numerical Prediction of the Round Jet in a Co-Flowing Stream by Three-Dimensional Vortex Method, Int. J. Turbo and Jet Engines, Vol.20 (2003), pp.235–244.

(26) Oster, D. and Wygnanski, I., The Forced Mixing Layer between Parallel Streams, J. Fluid Mech., Vol.123 (1982), pp.91–130.